Hindawi
Journal of Nanomaterials
Volume 2023, Article ID 1701496, 10 pages
https://doi.org/10.1155/2023/1701496

Research Article

Effect of Hydrothermal Reaction Temperature on Fluorescent Properties of Carbon Quantum Dots Synthesized from Lemon Juice for Adsorption Applications

Gadisa Deme,[1] Abebe Belay,[1] Dinsefa Mensur Andoshe,[2] Gemechu Barsisa,[1] Diriba Tsegaye,[1] Solomon Tiruneh,[1] and Cherinet Seboka[3]

[1]*Department of Applied Physics, Adama Science and Technology University, School of Applied Natural Science, P.O. Box 1888, Adama, Ethiopia*
[2]*Department of Material Science and Engineering, Adama Science and Technology University, School of Mechanical, Chemical and Material Engineering, P.O. Box 1888, Adama, Ethiopia*
[3]*Department of Physics, Madda Walabu University, College of Natural and Computational Sciences, P.O. Box 247, Robe, Ethiopia*

Correspondence should be addressed to Abebe Belay; abebebelay96@gmail.com

Received 11 August 2022; Revised 29 October 2022; Accepted 8 November 2022; Published 4 January 2023

Academic Editor: Kaliannan Durairaj

Photoluminescent carbon quantum dots (CQDs) were synthesized from lemon juice precursors via single-step, hydrothermal techniques under different temperatures to control the optical properties. The synthesized CQDs were characterized by PL, illuminated UV analyzer chamber, UV–vis spectroscopy, X-ray diffractometer, Fourier-transformed infrared spectrophotometry, and zeta potential techniques. The results show that the synthesized CQDs had an excellent blue–green emission extending up to the infrared region with high quantum yield (Φ) in the range of 14%–41%. The effect of reaction temperature and the aging of CQDs on the emission spectra of CQDs are also investigated. Furthermore, the adsorption effect of the synthesized CQDs was evaluated on methylene blue (MB) dyes. The result indicated the synthesized CQDs have excellent adsorbent properties with a removal efficiency of 60%–82% and an extremely fast adsorption rate of $6 \times 10^{-2}\,\text{min}^{-1}$ for MB dyes.

1. Introduction

Carbon quantum dots (CQDs) have received considerable attention from the scientific community due to their unique properties such as highly photoluminescent, excitation wavelength-dependent emission, large surface area, multifunctional groups, highly water solubility, high quantum yield (Φ), low toxicity, eco-friendly, nanoscale size, quasi-spherical shaped nanomaterials, and excellent biocompatibility [1]. Because of their unique properties, they have been applied in various areas such as biomedical [2], sensing [3], bioimaging [4], photocatalytic activity [5], adsorption [6], optoelectronics [7], and metal ions detection application [8].

There are two main approaches to the synthesis of CQDs, top-down and bottom-up [9]. The top-down approach refers to the breakdown of large carbon structures into nanoscale particles [10]. While the bottom-up approach refers to the synthesis of the CQDs from small organic molecules [11]. The hydrothermal bottom-up methods have become the most widely utilized technique in comparison with other methods as it is a simple operation, cost-effective, and eco-friendly [12].

Generally, the synthesis of CQDs involves the carbonization of carbon sources. CQDs can be synthesized from any carbon-containing materials, and their fluorescence properties are dependent on the precursor materials [13]. For instance, CQDs were synthesized from orange juice [14], apple juice [15], carrot juice [16], rice bran [17], orange peel [18], lemon peel [19], and *Elettaria cardamomum* [20]. The synthesis of CQDs from a natural carbon source like lemon juice is more attractive because it reduces chemical exposure (nontoxicity), is cheap, contains a renewable source of carbon, highly abundant biomass, amino-group enriched natural material, and has the potential to scale up. Also, the CQDs

are potential competitors to traditional metal-based semiconductor quantum dots such as TiO_2, Cd, and ZnO owing to their extremely interesting properties, such as biocompatibility, eco-friendly, recyclability of the adsorbent properties, and easy to synthesis [21]. The high specific surface area, excellent aqueous stability, large pore volume, and other properties make it preferable for adsorption applications. In general, C-dots have similar characteristics to heavy metal-based quantum dots but have a number of advantages such as good solubility in water, cheap starting materials, not contain heavy metals, efficient synthetic process, having strong photoluminescence properties, low toxicity, and good photostability [22].

The functional groups such as carbonyl (–C=O), carboxylic (–COOH), hydroxyl (–OH), and amine (–NH) on the surface of organic precursors are highly significant in the synthesis of CQDs [23]. The presence of such numerous functional groups on the surface of CQDs improves the fluorescent emission, water solubility, functionalization, and increases the surface activity, and results in different absorption behavior. These functional groups are also affected by reaction temperature and other factors. For the last several years, intensive research efforts have been devoted by the scientific community to better understanding of the structural, photophysical, and chemical properties of CQDs. However, the complete characterization of CQDs remains challenging. This is owing to the reality that CQDs products exist as a complex mixture comprising components with different sizes, distinctive surface functionalities, and complex mixtures. CQDs samples only represent the average properties of all individual CQDs [24]. Synthesized CQDs, with an excellent blue–green emission extending up to the infrared region with high quantum yield (Φ), have a significant function because it determines the selectivity and sensitivity has high application in the photocatalytic activities.

Several researches have been conducted to the synthesis of CQD from natural resources. For example, the quantum yield of C-dots derived from orange juice reported by Wang and Hu [14] is 26%. Similarly, the quantum yield obtained from lemon and apple juices [25] are 6.4% and 14.86%–24.89%, respectively. Most of the bottom-up synthesis approaches need several steps and strong acids, and posttreatment with surface passivation agents is essential to improve their water solubility and luminescence property. In this research, for the first time high amount of quantum yield of CQD synthesis from lemon juice using single step and applied for the adsorption effect on methylene blue (MB) dyes.

Therefore, the objectives of this research are to obtain a high amount of quantum efficiency of CQDs, which depend on hydrothermal reaction temperature via single step for adsorption applications. The synthesized CQDs have eco-friendly, better biocompatibility, highly water-soluble, and highly photoluminescent properties. In addition, they are widely distributed with several attractive features, including excellent photostability, lower toxicity, simple surface functionalization, and greater chemical stability.

2. Materials and Methods

2.1. Synthesis Methods of Fluorescent Carbon Quantum Dots. Fluorescent CQDs were synthesized from lemon juice using simple hydrothermal techniques at different temperatures (160, 180, and 200°C) for 6 hr reaction time. The lemon fruits were purchased from a local market (Adama, Ethiopia) and washed properly with clean water in order to remove dust and unwanted particles on the lemon surface. 13 ml of lemon juice solution was mixed with 7 ml of deionized water. The mixtures were stirred for 10 min using a magnetic stirrer at room temperature. The solution was transferred into a 25 ml autoclave and sealed seriously with teflon-lined stainless steel for hydrothermal reaction process [26]. After reaction temperature, dark brownish product was obtained. Large particles of impurities are removed to obtain nanoscale CQDs. The best purification techniques are the combinations of centrifuges and filter paper. The brown color solution was centrifuged at 5,000 rpm for 20 min to remove the impurity or large particles and filtered through 0.45 μm filter paper. Figure 1 shows the schematic fabrication mechanism of CQDs from lemon juice using hydrothermal methods.

2.2. Characterization Methods. The C-quantum dot sizes were determined using X-ray diffractometer (XRD-7000, X-ray diffractometer, MAXIma, SHIMADZU Corporation. Japan), which is equipped with Cu Kα_1 radiation ($\lambda = 1.5406$ Å) and operated at the voltage of 40 kV and current of 30 mA with a scanning speed of 3.00°/min. The samples data were collected in the range of $2\theta = 10° \leq 2\theta° \leq 80°$. The average crystalline particle size of CQDs is calculated using the relation expressed in Equations (1) and (2). The crystal structure diffraction is based on Wulf–Bragg's law shown in Equation (1) [27].

$$n\,\lambda = 2d\,\sin\theta, \tag{1}$$

where n is the order of diffraction (usually $n = 1$), λ is the X-ray wavelength, and d is the spacing between planes of given Miller indices h, k, and l, and θ is angle of diffraction.

The average crystallite size of CQDs calculated using Debye–Scherrer's Equation (2) [28].

$$D = \frac{K\lambda}{\beta_{hkl}(\cos\theta)}, \tag{2}$$

where D (nm) is the average crystallite size of the particle, λ (1.5406 Å) is the wavelength of the incident X-ray, β is the angular peak width that is half the maximum value in radians, and θ is the Bragg diffraction angle. The average crystallite sizes (D) are usually calculated from the most intense peak in the XRD pattern.

The UV–vis absorption spectra were obtained using UV–vis spectroscopy (MODEL-JASCO V-770, Japan) in the wavelength region of 200–800 nm at room temperature. The absorbance of CQDs was measured using 1 cm quartz cuvette. Equation (3) was used to compute the energy bandgap of the fabricated CQDs. The bandgap energy is determined by substituting the value of the

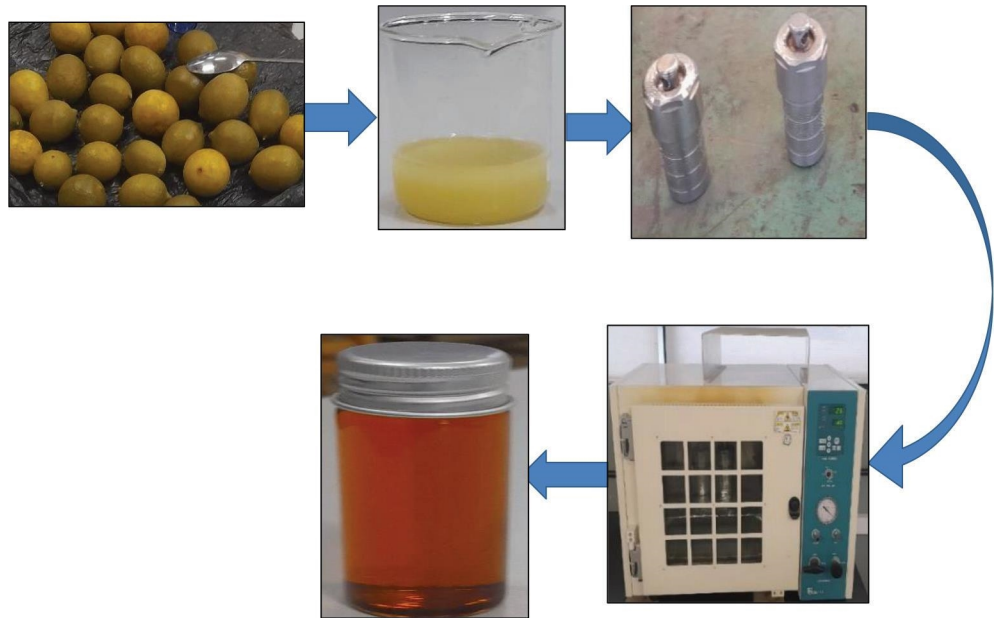

Figure 1: A schematic diagram for the synthesis of CQDs from lemon juice using hydrothermal techniques.

maximum absorption peak at a given wavelength using Equation (3) [29].

$$E_g = E_2 - E_1 = h\nu = h\frac{c}{\lambda} = \frac{1.240}{\lambda_{max}}(\text{keV}), \quad (3)$$

where E_g is the bandgap energy (eV), h is Planck's constant (6.626×10^{-34} J s), c is the velocity of light (3×10^8 m/s), and λ is the wavelength (nm) of absorption onset.

Furthermore, the optical bandgap energy (E_g) is determined from a Tauc-plot of Equation (4) [30].

$$\alpha h\nu = A\,(h\nu - E_g)^n, \quad (4)$$

where α is the absorbance coefficient, h is Planck's constant; ν is the frequency of light radiation, and E_g is the bandgap energy where "n" takes the values of ½ allowed direct transition.

The fluorescence emission spectra of CQDs were recorded using a fluorescence spectrophotometer (Model, MY18490002, Cary Eclipse Fluorescence Spectrophotometer, Agilent Technologies, and Malaysia) at room temperature. The excitation wavelengths measured from 360 to 520 nm and their corresponding emission spectral shift toward higher wavelengths measured from UV–vis up to infrared regions. The quantum yield (Φ) of CQD is calculated, according to Equation (5) [31].

$$\Phi = \frac{\text{Photons emitted}}{\text{Photons absorbed}}. \quad (5)$$

However, the most common method employed to obtain Φ of CQDs is according to Equation (6) [32].

$$\Phi_{CQDs} = \Phi_{ref}\frac{I_{CQDs}}{I_{ref}}\frac{A_{ref}}{A_{CQDs}}\frac{(n_{CQDs})^2}{(n_{ref})^2}. \quad (6)$$

In Equation (6), MB ($\Phi = 0.52$) is used as the reference material and I refer to the integrated emission intensity curve of the sample and reference. Where A refers to the UV–vis absorption intensity of the sample and reference, and n refers to the refractive index of the solvents used for the sample (water = 1.333) and reference (ethanol = 1.3614) measurements.

A Fourier-transformed infrared (FT-IR) (Perkin Elmer, Spectrum 65 FT-IR) was used to study the functional groups attached to the CQD and measured in the wavenumber region of 4,000–400 cm^{-1}. Zeta potential is used to study the surface charge and photostability of fluorescent CQDs. The zeta potential investigation was carried out using the Zetasizer Nano series (Malvern) (Zetasizer Ver.8.02, MAL 1149420) [6].

2.3. Methods of Adsorption for Removal of Methylene Blue (MB) Dyes. Adsorption of MB (cationic ions) on CQDs included multiple adsorption mechanisms, such as electrostatic interactions, hydrogen bonds, and surface complexation between adsorbent and absorbent were carried out according to procedures of Chen et al. [33]. Electrostatic interactions may consider the significant adsorption mechanisms between CQDs-adsorbent and MB dye due to a mass of negatively charged oxygen and nitrogen-containing functional groups on the surface of CQDs. These negatively charged nitrogen and oxygen-containing functional groups on the surfaces of CQDs can provide active sites for MB dye adsorption [10]. To evaluate the kinetics of the adsorption process the experimental data were fitted to pseudo-first-order kinetic models. The organic dye removal efficiency of synthesized CQDs was evaluated by the

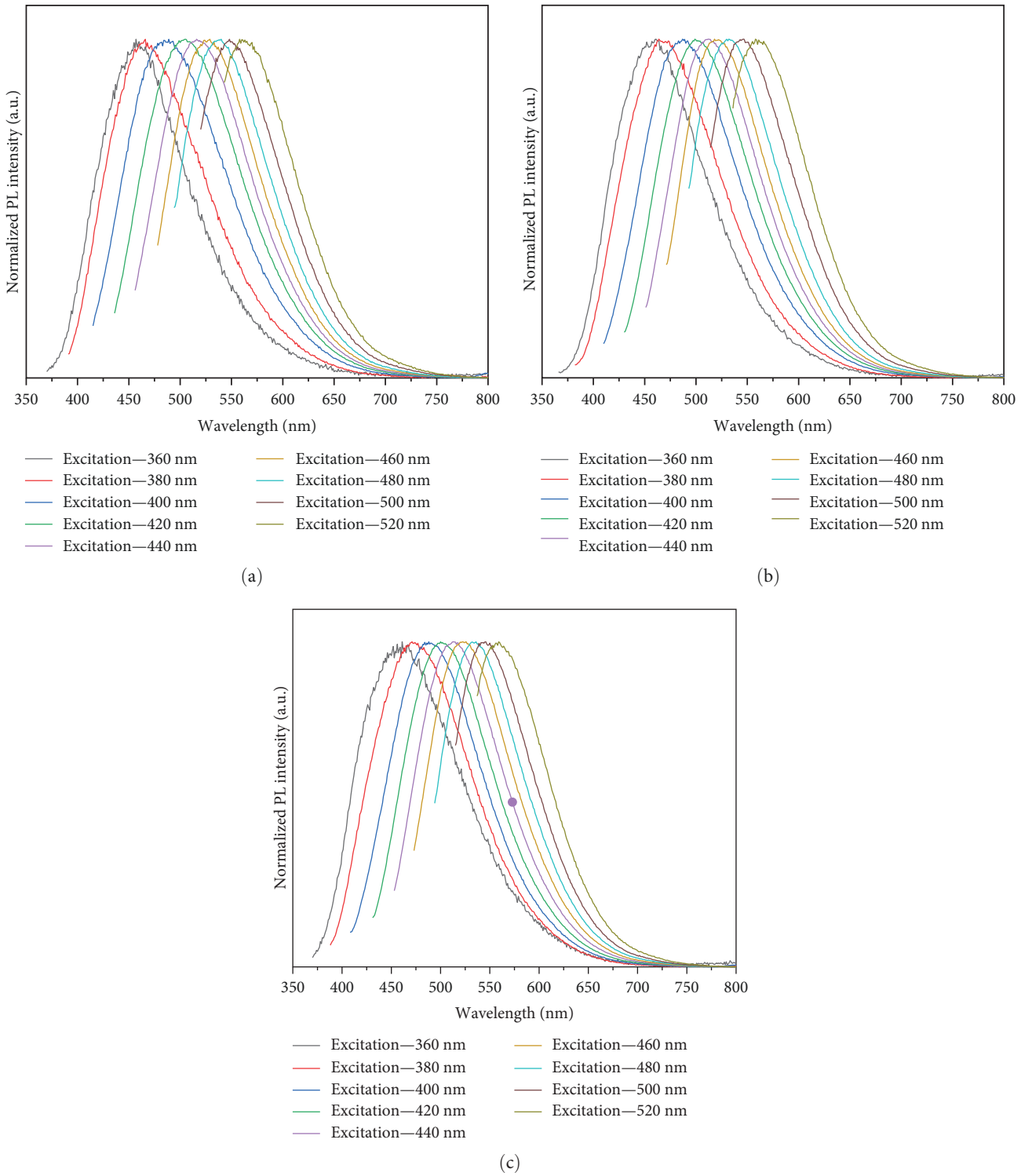

Figure 2: The normalized emission spectra of CQDs and their corresponding excitation wavelength synthesized at the temperature of (a) 160°C, (b) 180°C, and (c) 200°C.

adsorption of MB dye in aqueous solutions. Such applications are also important to remove dye from wastewater before discharging them into rivers or oceans.

Adsorption performances of fluorescent CQDs were investigated for removal of highly toxic MB dye. The adsorption studies were carried by adding 20 mg of CQDs into 0.01 mg/l concentration of MB in the 250 ml of conical flasks for contact time of 0–24 min at room temperature (25°C). The solution was stirred with 150 rpm for 24 min and the solution was measured at 3 min intervals. The removal efficiency ($R\%$) and the equilibrium adsorbed capacity q_e (mg/g) of the MB dye were measured using UV–vis spectroscopy.

The experimental studies were conducted to inspect the influences of contact time on MB adsorption.

The removal efficiency ($R\%$) and the equilibrium removal capacity q_e (mg/g) of the MB dye were computed using Equations (7) and (8) [34].

$$R\% = \left(1 - \frac{C_e}{C_0}\right) \times 100, \tag{7}$$

$$q_e = (C_0 - C_e) \times \frac{\nu}{m}, \tag{8}$$

where C_0 and C_e (mg/l) are the initial and equilibrium concentrations of absorbate (mg/l) in the solution, respectively; V (l) is the volume of dye solution, and m (g) is the weight of the adsorbent (CQDs).

According to the dynamic Langmuir–Hinshelwood model, the adsorption rate of organic dye of MB was computed according to the pseudo-first-order kinetic as shown in Equation (9) for very dilute solution [35].

$$\ln\left[\frac{C_0}{C_e}\right] = k_t, \tag{9}$$

where C_0 and C_e should be the equilibrium concentration of dye adsorption and the concentration of dye after contact time t, respectively. For calculation purposes, here, C_0 and C_e are taken as the absorbance of the dyes at time zero and the absorbance of the dyes after adsorption time t, respectively; k stands for the dye adsorption rate.

3. Results and Discussion

3.1. Photoluminescence Analysis. Photoluminescence properties of CQDs are the signature and the most important property from their application point of view. The emission spectra of CQDs were obtained at various temperatures for 6 hr reaction time as illustrated in Figure 2. The results indicated the CQDs synthesized at the mentioned temperatures have an emission spectrum of blue and green extending to the infrared region [36]. Depending on the hydrothermal temperature, the emission peak extends from blue–green region to infrared region and all these peaks confirm that the synthesized CQDs are dependent on excitation wavelength. The CQDs synthesized at 160°C have longer Stock shift than the other synthesis at temperatures of 180 and 200°C. This longer shift is due to the effects of functional groups attached to CQDs and the results may be due to temperature effects. The peak emission spectra are typically depending on temperature, size, and functional groups [37]. In this research, although the CQDs were synthesized under the same hydrothermal conditions, the sizes of the synthesized CQDs were different. This may be due to the various degradation temperatures of the precursors allowing them to nucleate at different conditions, thus forming different-sized CQDs nanomaterials [38].

The tunable fluorescence emissions of CQDs originate from the oxide-related surface effects and quantum confinement is the responsible mechanism due to the presence of functional groups [38]. Quantum yield is an important parameter that characterizes luminescent nanomaterials. The easiest method to determine quantum yield involves comparing the luminescent intensity of the sample with the standard compound. The quantum yields (Φ) of CQDs calculated according to Equation (6) are 24%, 14%, and 41% at the temperature of 160, 180, and 200°C, respectively. The results could be attributed to the effective conversion of natural constituents into carbonization by increasing the hydrothermal temperature of the process. This means, according to our results, the higher temperature of 200°C has the optimum reaction temperature for maximum emission. Previously it has been reported that the quantum yield obtained from various natural resources are within the range of 6.4%–26% and the higher temperature yield a high amount of maximum emission [14]. Also, CQDs with longer emission wavelengths have low QY due to loss of energy were observed. Moreover, reaction time is also the other factor that affects the PL intensity of the CQDs. The CQDs are synthesized at different reaction times 2, 4, 6, and 8 hr at 160°C temperature shown in Figure 3. Increases of hydrothermal reaction time result in increases in the intensity of emission spectra. The longer hydrothermal reaction time leads to increase the conversion of constituents into carbonization and reason for increased intensity. The CQDs synthesized at 8 hr have more intensity meaning the quantum yield (Φ) at this reaction time is maximum. On the other hand, at shorter times especially for less than 4 hr the complete carbonization process is small as results less quantum yield obtained. These results are quite similar with the previously reported by Hoan et al. [25].

The other factor that influences the emission intensity of synthesis CQDs is the aging time. Figure 4 shows the

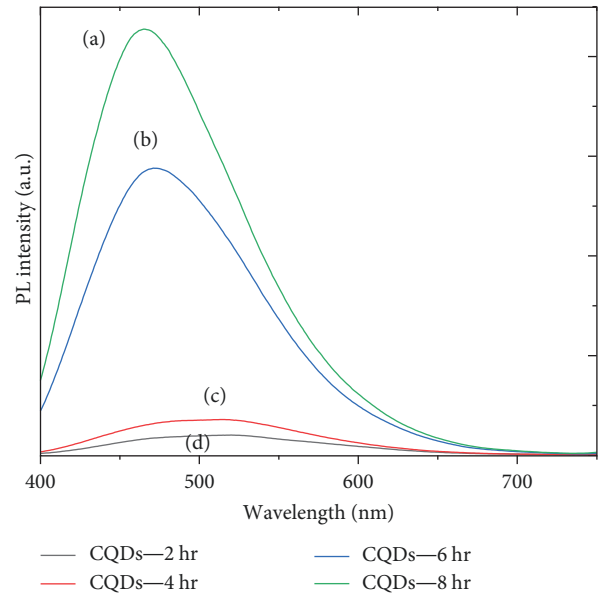

Figure 3: Emission spectra of CQDs synthesized at the temperature of 160°C and different hydrothermal reaction times (a) 8, (b) 6, (c) 4, and (d) 2 hr.

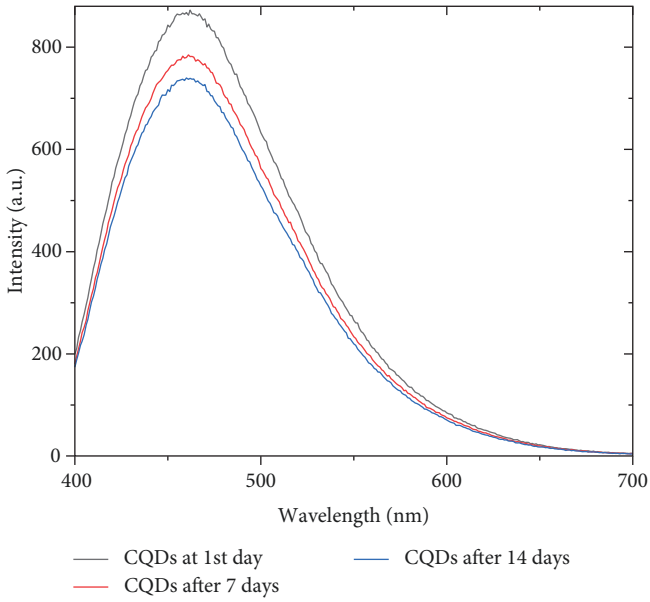

Figure 4: The emission intensity of CQDs measured at different aging times: 1st, 7th, and 14th day, respectively.

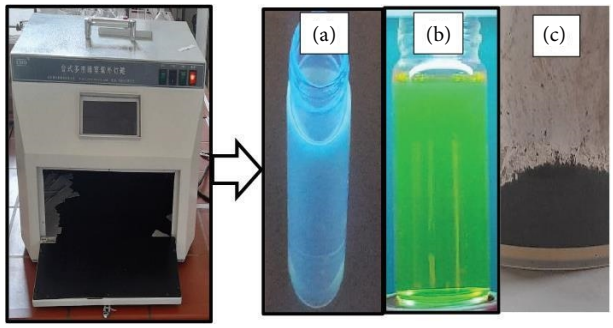

Figure 5: CQDs illuminated by (a) UV light at the wavelength of 254 nm and emit blue color, (b) UV light at the wavelength of 365 nm and emit green color, and (c) excitation with visible color emit dark brown (600 nm). It means that as excitation wavelength increasing the emission wavelength shift to higher wavelength.

emission intensity of synthesized CQDs at different aging times (1st, 7th, and 14th day) after synthesis. The intensity of the emission decreases as the aging time increases. The surface state of synthesized CQDs is a significant factor that determines the emission intensity. The other factors degrading the constituents of CQDs are the movement and temperature of the surrounding environment. Figures 5(a) and 5(b) show CQDs placed under UV analyzer illuminated by wavelengths of 254 and 365 nm. Blue and green emissions were observed for 254 and 365 nm, respectively, which confirm the presence of CQDs. Similarly, a dark brown (Figure 5(c)) emission was obtained when illuminated by visible light.

3.2. UV–Vis Absorption Spectra Analysis. Figure 6(a) shows the UV–vis absorption spectra of CQDs synthesized at the temperature of 160°C. It has two absorption maxima at 217 and 282 nm, respectively. The bands are corresponding to –C=O and C=C due to n–π^* and π–π^* transitions, respectively.

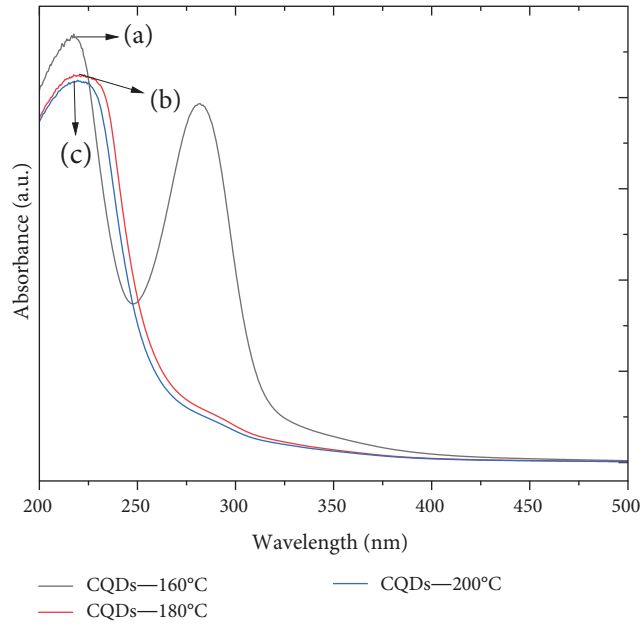

Figure 6: UV–Vis absorption spectra of CQDs prepared at the temperature of (a) 160°C, (b) 180°C, and (c) 200°C, respectively.

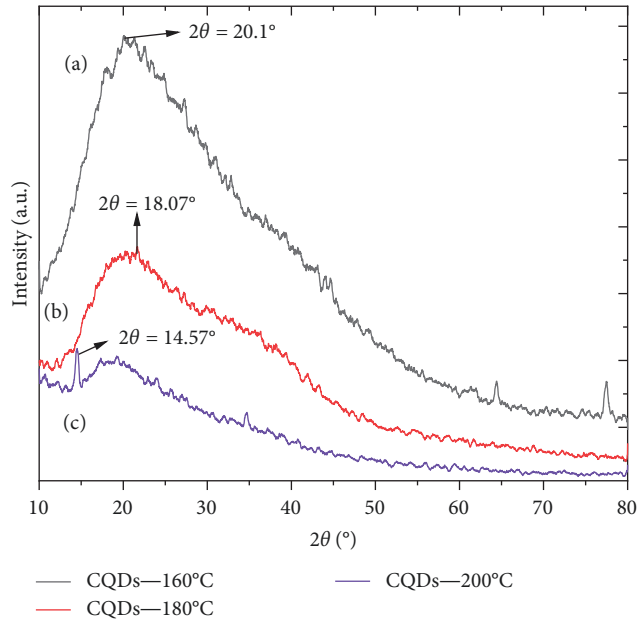

Figure 7: XRD diffraction spectra of CQDs synthesized at (a) 160°C, (b) 180°C, and (c) 200°C.

These results are similar to previously reported CQDs synthesized from leaves of *E. cardamomum* [20]. The UV–vis absorption spectrum of the C-quantum dot has no background absorption in the visible area. This result demonstrated that there are no other forms of nanocarbon produced during the partial carbonization of the precursors, which are usually absorbed at longer wavelengths. The nonuniform size distribution and functional groups of CQDs were responsible for the appearance of two absorption maxima. On the other hand, the absorption peaks for 180 and

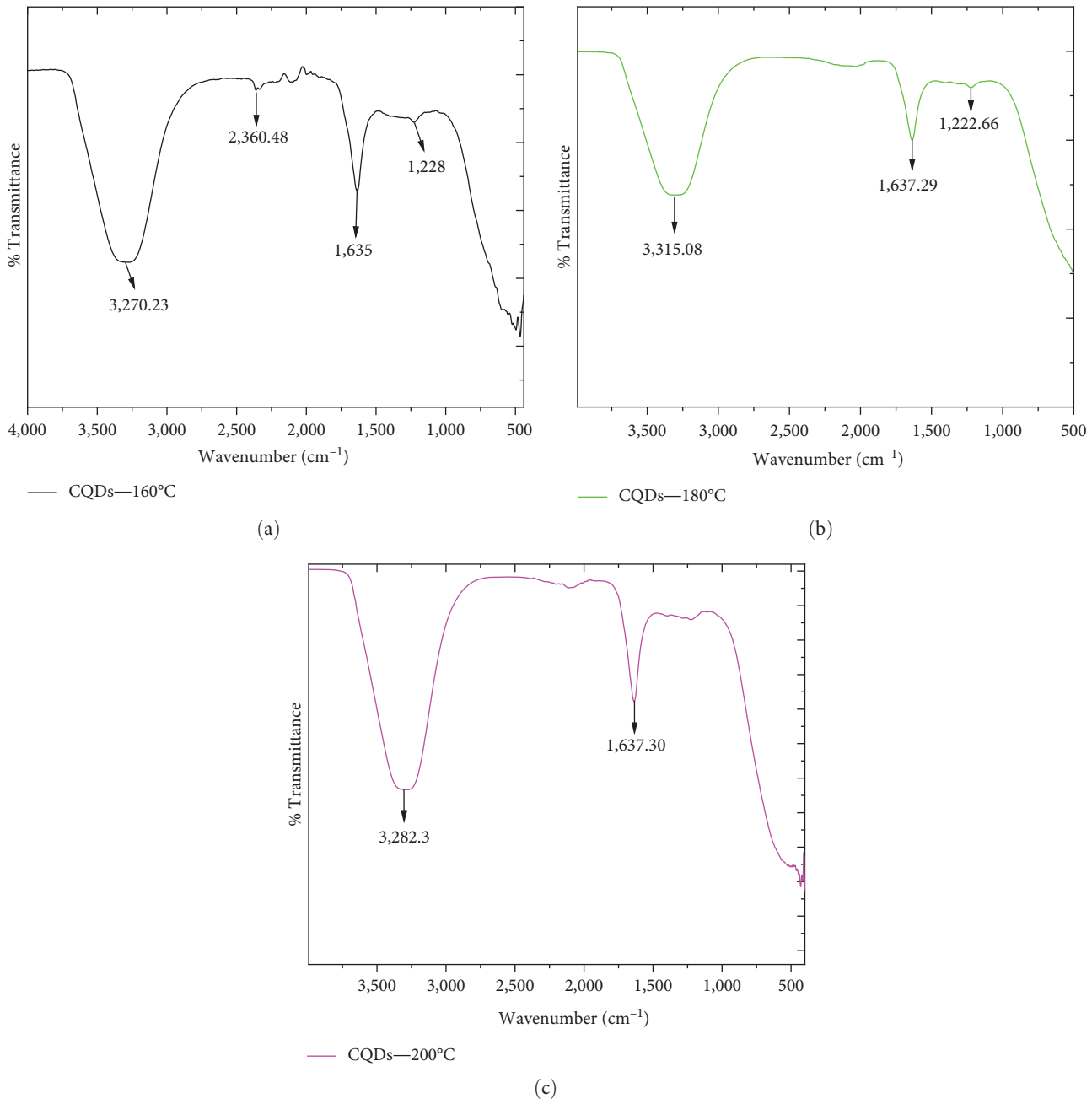

Figure 8: The FT-IR spectra of CQDs synthesized at the temperature of (a) 160°C, (b) 180°C, and (c) 200°C.

200°C temperatures are 222 and 219.5 nm, respectively. Only one peak occurs at 180 and 200°C indicating the uniform size particle as the temperature increases. In general, the synthesized CQDs have strong optical absorption in the UV region with a tail extending to the visible range. Also, the CQDs synthesized at 160°C have higher bandgap energy and these results confirm the previously reported results, synthesized CQDs via a one-step laser-passivation method [39]. The calculated bandgap energy at the temperature at 180 and 200°C are 4.6 and 4.68 eV, respectively.

3.3. X-Ray Diffraction Analysis. An X-ray diffraction study has been carried out to investigate the crystal structure of the synthesized CQDs. Figure 7 shows XRD patterns of CQDs synthesized at different temperatures of 160, 180, and 200°C under hydrothermal treatment. The result indicates that the XRD pattern exhibits a wide diffraction peak at $2\theta = 20.1°$, 18.07°, and 14.57°, for 160, 180, and 200°C, respectively. From XRD results the intensity peaks decrease as the temperature of hydrothermal increases; this is due to the disordered carbon atoms CQDs as the temperature increases.

3.4. Fourier Transform Infra-Red Analysis. The FT-IR spectrum of the CQDs fabricated from lemon juice contains different functional groups such as carbonyl, amine, aromatic ester, hydroxyl, and carboxylic acid groups as shown

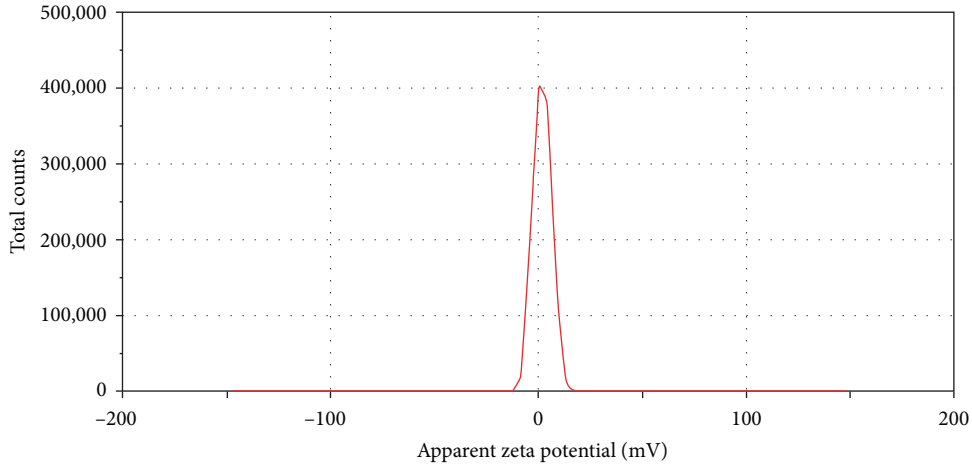

Figure 9: Zeta potential of CQDs synthesized at 160°C.

in Figure 8. The water solubility of the synthesized CQDs is high, due to the presence of organic functional groups like C=O or oxygen-containing functional groups on the surface of the CQDs [26]. Figure 8(a)–8(c) is the FT-IR spectra of CQD synthesized at the temperatures of 160, 180, and 200°C, respectively. All the CQDs samples contain functional group C=O due to stretching at 1,635, 1,637, and 1,637 cm^{-1} and these are fundamental properties of CQDs. CQDs synthesized at 160°C exhibits more absorption peaks at 3,270, 2,360, 1,635, and 1,228 cm^{-1} corresponding to the vibrational of N–H/OH, COOH, C=O, and C–O functional groups, respectively, comparable with report [40]. Also, the CQDs synthesized at 180°C exhibit absorption peaks at 3,315 (–NH/OH), 1,637 (C=O), and 1,222 cm^{-1} (C–O). Similarly, the CQDs synthesized at 200°C exhibit absorption peaks at 3,282 (–NH/OH), and 1,637 (C=O) cm^{-1}. Only a few peaks appeared for CQDs synthesized at 180 and 200°C indicating many of the functional groups disappeared due to the increase in the temperature.

3.5. Zeta Potential. The other properties of CQDs are investigated by zeta potential shown in Figure 9. The CQDs have a positive charge due to the presence of a large density of amine groups as confirmed on FT-IR spectra of Figure 9(a)–9(c). The obtained zeta potential result shows that the CQDs have potential of ~1.55 mV, which suggests relatively neutral and good stability [25].

3.6. Applications CQDS for Removal of Methylene. Figure 10 absorbance versus wavelength of MB dyes in the presence of CQDs at different time intervals. The good water solubility and excellent physicochemical properties of CQDs in the presence of negatively charged nitrogen elements, carboxylic acid (COOH), and other oxygen-containing functional groups on the surface serve as active sites of adsorption of MB dyes. Furthermore, electrostatic interactions, ionic exchange, and hydrogen bonding may occur between CQDs adsorbent and adsorbate (MB) dyes. The removal efficiency ($R\%$) versus time of MB dye by

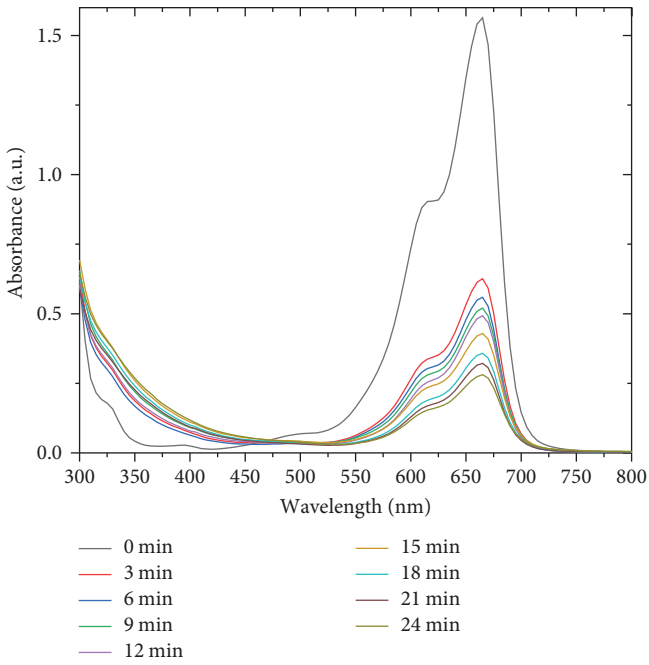

Figure 10: Absorbance versus wavelength of methylene blue dyes in the presence of CQDs at different time intervals.

CQDs is shown in Figure 11. Due to the large surface area and contact time of CQDs, the surface adsorption capacity of the CQDs for removing MB dyes is high. The CQDs adsorb efficiency is 60%–82% within the time interval of 3–24 min, respectively. The contact time indicates that the optimum adsorption was 24 min with removal efficiency ($R\%$) of 82%. From the kinetic point, the calculated rate constant of the removal reaction is shown in Figure 12. The adsorption removal reaction is considered a pseudo-first-order kinetic reaction. The rate constant for adsorption at maximum wavelength of MB is 6.0×10^{-2} min^{-1} with efficiency of 60%–82%.

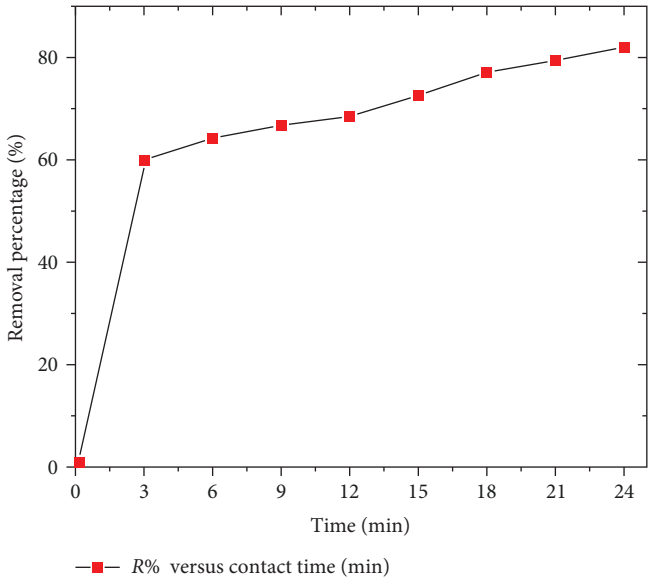

Figure 11: Removal efficiency ($R\%$) versus time of methylene blue dye by CQDs.

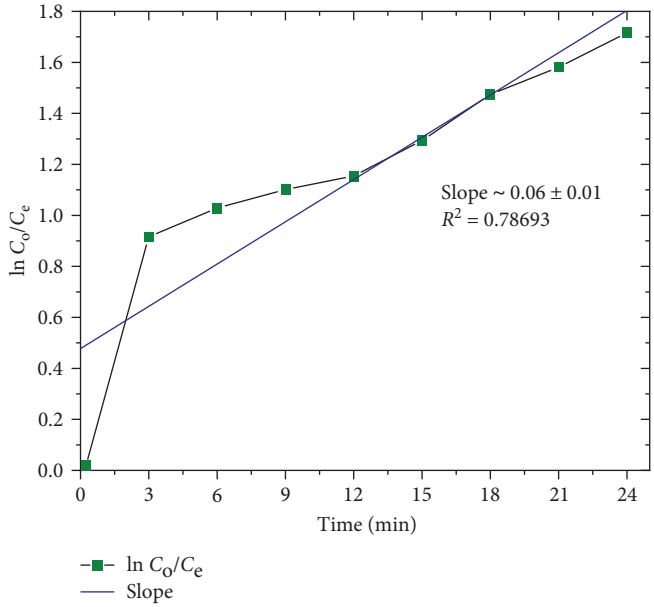

Figure 12: The rate of adsorption removal of methylene blue (MB) catalyzed by carbon quantum dots (CQDs) nanomaterials (20 mg/100 ml).

4. Conclusions

In this work, CQDs were synthesized via simple, low cost, and one-step hydrothermal methods from cheap, eco-friendly, and easily available lemon juice under different temperatures. To determine the fundamental properties of CQDs, different characterization techniques such as illumination UV light analyzer, XRD, UV–vis, PL, FT-IR, and zeta potential were utilized. The obtained results show that the synthesized CQDs had an excellent blue–green emission extending up to the infrared region and also depended on reaction time with a high quantum yield (Φ) in the range of 14%–41%. The reaction temperature and aging have an effect on the fluorescent properties of CQDs. The study result also indicated that the CQDs are excellent adsorbents for the effective adsorption of MB with a removal efficiency of 82%.

Data Availability

All data in detail are available when they are required.

Conflicts of Interest

The authors declare that they have no conflicts of interest.

Acknowledgments

This work is financially supported by the Adama Science and Technology University and the Ministry of Innovation and Technology of Ethiopia. The authors would like to acknowledge ASTU and MINT for the support.

References

[1] R. M. El-Shabasy, M. Farouk Elsadek, B. Mohamed Ahmed, M. Fawzy Farahat, K. N. Mosleh, and M. M. Taher, "Recent developments in carbon quantum dots: properties, fabrication techniques, and bio-applications," *Processes*, vol. 9, no. 2, Article ID 388, 2021.

[2] N. Azam, M. Najabat Ali, and T. Javaid Khan, "Carbon quantum dots for biomedical applications: review and analysis," *Frontiers in Materials*, vol. 8, Article ID 700403, 2021.

[3] N. A. A. Nazri, N. H. Azeman, Y. Luo, and A. A. A. Bakar, "Carbon quantum dots for optical sensor applications: a review," *Optics & Laser Technology*, vol. 139, Article ID 106928, 2021.

[4] R. Atchudan, S. Chandra Kishore, P. Gangadaran et al., "Tunable fluorescent carbon dots from biowaste as fluorescence ink and imaging human normal and cancer cells," *Environmental Research*, vol. 204, Part D, Article ID 112365, 2022.

[5] Z. Zhang, T. Zheng, X. Li, J. Xu, and H. Zeng, "Progress of carbon quantum dots in photocatalysis applications," *Particle & Particle Systems Characterization*, vol. 33, no. 8, pp. 457–472, 2016.

[6] M. Yahaya Pudza, Z. Zainal Abidin, S. Abdul Rashid, F. Md Yasin, A. S. M. Noor, and M. A. Issa, "Eco-friendly sustainable fluorescent carbon dots for the adsorption of heavy metal ions in aqueous environment," *Nanomaterials*, vol. 10, no. 2, Article ID 315, 2020.

[7] E. A. Stepanidenko, E. V. Ushakova, A. V. Fedorov, and A. L. Rogach, "Applications of carbon dots in optoelectronics," *Nanomaterials*, vol. 11, no. 2, Article ID 364, 2021.

[8] X. Gao, C. Du, Z. Zhuang, and W. Chen, "Carbon quantum dot-based nanoprobes for metal ion detection," *Journal of Materials Chemistry C*, vol. 4, no. 29, pp. 6927–6945, 2016.

[9] R. Atchudan, T. N. J. I. Edison, S. Perumal, N. Muthuchamy, and Y. R. Lee, "Hydrophilic nitrogen-doped carbon dots from biowaste using dwarf banana peel for environmental and biological applications," *Fuel*, vol. 275, Article ID 117821, 2020.

[10] C. Long, Z. Jiang, J. Shangguan, T. Qing, P. Zhang, and B. Feng, "Applications of carbon dots in environmental pollution control: a review," *Chemical Engineering Journal*, vol. 406, Article ID 126848, 2021.

[11] F. Du, J. Li, Y. Hua et al., "Multicolor nitrogen-doped carbon dots for live cell imaging," *Journal of Biomedical Nanotechnology*, vol. 11, no. 5, pp. 780–788, 2015.

[12] X. Lin, M. Xiong, J. Zhang et al., "Carbon dots based on natural resources: synthesis and applications in sensors," *Microchemical Journal*, vol. 160, Part A, Article ID 105604, 2021.

[13] V. Sharma, P. Tiwari, and S. M. Mobin, "Sustainable carbon-dots: recent advances in green carbon dots for sensing and bioimaging," *Journal of Materials Chemistry B*, vol. 5, no. 45, pp. 8904–8924, 2017.

[14] Y. Wang and A. Hu, "Carbon quantum dots: synthesis, properties and applications," *Journal of Materials Chemistry C*, vol. 2, no. 34, pp. 6921–6939, 2014.

[15] V. N. Mehta, S. Jha, H. Basu, R. K. Singhal, and S. K. Kailasa, "One-step hydrothermal approach to fabricate carbon dots from apple juice for imaging of mycobacterium and fungal cells," *Sensors and Actuators B: Chemical*, vol. 213, pp. 434–443, 2015.

[16] Y. Liu, Y. Liu, M. Park et al., "Green synthesis of fluorescent carbon dots from carrot juice for in vitro cellular imaging," *Carbon Letters*, vol. 21, pp. 61–67, 2017.

[17] V. K. Jothi, K. Ganesan, A. Natarajan, and A. Rajaram, "Green synthesis of self-passivated fluorescent carbon dots derived from rice bran for degradation of methylene blue and fluorescent ink applications," *Journal of Fluorescence*, vol. 31, pp. 427–436, 2021.

[18] X. Hu, Y. Li, Y. Xu et al., "Green one-step synthesis of carbon quantum dots from orange peel for fluorescent detection of *Escherichia coli* in milk," *Food Chemistry*, vol. 339, Article ID 127775, 2021.

[19] A. Tyagi, K. M. Tripathi, N. Singh, S. Choudhary, and R. K. Gupta, "Green synthesis of carbon quantum dots from lemon peel waste: applications in sensing and photocatalysis," *RSC Advances*, vol. 6, no. 76, pp. 72423–72432, 2016.

[20] M. Zaib, A. Akhtar, F. Maqsood, and T. Shahzadi, "Green synthesis of carbon dots and their application as photocatalyst in dye degradation studies," *Arabian Journal for Science and Engineering*, vol. 46, no. 1, pp. 437–446, 2021.

[21] A. Sharma and J. Das, "Small molecules derived carbon dots: synthesis and applications in sensing, catalysis, imaging, and biomedicine," *Journal of Nanobiotechnology*, vol. 17, Article ID 92, 2019.

[22] S. Sugiarti and N. Darmawan, "Synthesis of fluorescence carbon nanoparticles from ascorbic acid," *Indonesian Journal of Chemistry*, vol. 15, no. 2, pp. 141–145, 2015.

[23] S. Das, L. Ngashangva, and P. Goswami, "Carbon dots: an emerging smart material for analytical applications," *Micromachines*, vol. 12, no. 1, Article ID 84, 2021.

[24] Q. Hu, X. Gong, L. Liu, and M. M. F. Choi, "Characterization and analytical separation of fluorescent carbon nanodots," *Journal of Nanomaterials*, vol. 2017, Article ID 1804178, 23 pages, 2017.

[25] B. T. Hoan, P. D. Tam, and V.-H. Pham, "Green synthesis of highly luminescent carbon quantum dots from lemon juice," *Journal of Nanotechnology*, vol. 2019, Article ID 2852816, 9 pages, 2019.

[26] B. T. Hoan, P. Van Huan, H. N. Van et al., "Luminescence of lemon-derived carbon quantum dot and its potential application in luminescent probe for detection of Mo^{6+} ions," *Luminescence*, vol. 33, no. 3, pp. 545–551, 2018.

[27] S. P. Smrithi, N. Kottam, and B. R. Vergis, "Heteroatom modified hybrid carbon quantum dots derived from *Cucurbita pepo* for the visible light driven photocatalytic dye degradation," *Topics in Catalysis*, 2022.

[28] Z. Yu, L. Zhang, X. Wang, D. He, H. Suo, and C. Zhao, "Fabrication of ZnO/carbon quantum dots composite sensor for detecting no gas," *Sensors*, vol. 20, no. 17, Article ID 4961, 2020.

[29] Y. Zhou, E. M. Zahran, B. A. Quiroga et al., "Size-dependent photocatalytic activity of carbon dots with surface-state determined photoluminescence," *Applied Catalysis B: Environmental*, vol. 248, pp. 157–166, 2019.

[30] J. Jumardin, A. Maddu, K. Santoso, and I. Isnaeni, "Synthesis of carbon dots (CDs) and determination of optical gap energy with Tauc plot method," *Jambura Physics Journal*, vol. 3, no. 2, pp. 73–86, 2021.

[31] K. J. Mintz, Y. Zhou, and R. M. Leblanc, "Recent development of carbon quantum dots regarding their optical properties, photoluminescence mechanism, and core structure," *Nanoscale*, vol. 11, no. 11, pp. 4634–4652, 2019.

[32] I. Alkian, H. Sutanto, and Hadiyanto, "Quantum yield optimization of carbon dots using response surface methodology and its application as control of Fe^{3+} ion levels in drinking water," *Materials Research Express*, vol. 9, no. 1, Article ID 015702, 2022.

[33] Q. Chen, H. Wang, X. Tang et al., "One-step synthesis of carbon quantum dot-carbon nanotube composites on waste eggshell-derived catalysts for enhanced adsorption of methylene blue," *Journal of Environmental Chemical Engineering*, vol. 9, no. 5, Article ID 106222, 2021.

[34] M. Maruthapandi, V. B. Kumar, and A. Gedanken, "Carbon dot initiated synthesis of poly(4,4′-diaminodiphenylmethane) and its methylene blue adsorption," *ACS Omega*, vol. 3, no. 6, pp. 7061–7068, 2018.

[35] Z. Peng, Y. Zhou, C. Ji et al., "Facile synthesis of "boron-doped" carbon dots and their application in visible-light-driven photocatalytic degradation of organic dyes," *Nanomaterials*, vol. 10, no. 8, Article ID 1560, 2020.

[36] M. Jorns and D. Pappas, "A review of fluorescent carbon dots, their synthesis, physical and chemical characteristics, and applications," *Nanomaterials*, vol. 11, no. 6, Article ID 1448, 2021.

[37] M. Farshbaf, S. Davaran, F. Rahimi, N. Annabi, R. Salehi, and A. Akbarzadeh, "Carbon quantum dots: recent progresses on synthesis, surface modification and applications," *Artificial Cells, Nanomedicine, and Biotechnology*, vol. 46, no. 7, pp. 1331–1348, 2018.

[38] M. S. Ghamsari, A. M. Bidzard, W. Han, and H.-H. Park, "Wavelength-tunable visible to near-infrared photoluminescence of carbon dots: the role of quantum confinement and surface states," *Journal of Nanophotonics*, vol. 10, no. 2, Article ID 026028, 2016.

[39] X. Wang, Y. Feng, P. Dong, and J. Huang, "A mini review on carbon quantum dots: preparation, properties, and electrocatalytic application," *Frontiers in Chemistry*, vol. 7, Article ID 671, 2019.

[40] X. Miao, D. Qu, D. Yang et al., "Synthesis of carbon dots with multiple color emission by controlled graphitization and surface functionalization," *Advanced Materials*, vol. 30, no. 1, Article ID 1704740, 2018.